Proceedings of ASME Turbo Expo 2011
GT2011
June 6-10, 2011, Vancouver, British Columbia, Canada

GT2011-45401

Turbulent Consumption Speed Scaling of H_2/CO Blends

Prabhakar Venkateswaran
School of Aerospace Engineering

Andrew D. Marshall
School of Mechanical Engineering

David R. Noble
School of Aerospace Engineering

Jerry M. Seitzman
School of Aerospace Engineering

Tim C. Lieuwen
School of Aerospace Engineering

Georgia Institute of Technology
Atlanta, GA 30332-0150

ABSTRACT

This paper describes measurements and analysis of global turbulent consumption speeds, $S_{T,GC}$, of hydrogen/carbon monoxide (H_2/CO) mixtures. The turbulent flame properties of such mixtures are of fundamental interest because of their strong stretch sensitivity and of practical interest since they are the primary constituents of syngas fuels. Data are analyzed at mean flow velocities and turbulence intensities of $4 < U_0 < 50$ m/s and $1 < u'_{rms}/S_{L,0} < 100$, respectively, for H_2/CO blends ranging from 30-90% H_2 by volume. Data from two sets of experiments are reported. In the first, fuel blends ranging from 30-90% H_2 and mixture equivalence ratio, ϕ, were adjusted at each fuel composition to have nominally the same un-stretched laminar flame speed, $S_{L,0}$. In the second set, equivalence ratios were varied at constant H_2 levels. The data clearly corroborate results from other studies that show significant sensitivity of $S_{T,GC}$ to fuel composition. For example, at a fixed u'_{rms}, $S_{T,GC}$ of a 90% H_2 case (at $\phi = 0.48$) is a factor of three times larger than the baseline $\phi = 0.9$, CH_4/air mixture that has the same $S_{L,0}$ value. We also describe physics-based correlations of these data, using leading points concepts and detailed kinetic calculations of their stretch sensitivities. These results are used to develop an inequality for negative Markstein length flames that bounds the turbulent flame speed data and show that the data can be collapsed using the maximum stretched laminar flame speed, $S_{L,max}$, rather than $S_{L,0}$.

[*keywords:* syngas, hydrogen, turbulent flame speed, global consumption speed, Bunsen flames, leading points]

INTRODUCTION

There is significant interest in developing dry low NOx combustion technologies that can operate with synthetic gas (syngas) fuels derived from gasified coal or biomass [1]. Syngas fuels are typically composed primarily of H_2 and CO, and may also contain smaller amounts of CH_4, N_2, CO_2, H_2O, and other higher order hydrocarbons [1]. However, the specific composition depends upon the fuel source and processing technique, leading to substantial variability in composition.

A variety of operability, emissions, and structural life issues must be addressed in evaluating the impact of fuel composition on a gas turbine combustor; e.g., NOx and CO emissions, liner and fuel nozzle thermal loading, blow-off and flashback limits, and combustion instabilities. The turbulent flame speed is an important parameter through which the fuel composition exerts influences on many of these issues [2]. For example, the turbulent flame speed has a direct impact on the flame length and its spatial distribution in the combustor. This, in turn, affects the thermal loading distribution on the combustor liners, fuel nozzles and other hardware. Furthermore, the flames proclivity to flashback is directly a function of how rapidly the flame propagates into the reactants, which is dependent on the turbulent flame speed. In addition, the turbulent flame speed has an important influence on combustion instability limits through its influence upon the flame shape and length [3]. For example, measurements from Santavicca [4] have clearly shown how combustion instability boundaries are influenced by changes in flame location, due to changes in H_2 content of the fuel or mixture stoichiometry.

Numerous studies have discussed turbulent flame speed correlations of the form $S_T = S_{L,0} \cdot f(u'_{rms})$, where u'_{rms} denotes the root-mean-square (RMS) turbulence fluctuations [5-6]. However, u'_{rms} and $S_{L,0}$ alone do not capture many important characteristics of the turbulent flame speed [5]. It is also significantly affected by mean flow velocity [7], length scale [8-10], and fuel composition – it is this latter sensitivity which is a key focus of this study. For example, Kido *et al.* [11-12] obtained data for mixtures of H_2, methane (CH_4), and propane (C_3H_8) where, by adjusting the dilution and stoichiometries of the different fuel blends, they obtained different mixtures with the same un-stretched laminar flame speed, $S_{L,0}$. Their data clearly show that these mixtures have substantially different turbulent flame speeds, with the high H_2 mixtures having an order of magnitude larger S_T value than the propane mixture. Thus, two different fuel mixtures can have appreciably different turbulent flame speeds, despite having the same un-stretched laminar flame speed, turbulence intensity and burner configuration.

These fuels effects are believed to be associated with the stretch sensitivity of the reactant mixture which leads to variations in the local consumption speed along the turbulent flame front. In particular, the high mass diffusivity of H_2 makes syngas mixtures highly stretch sensitive. Stretch effects can be manifested through non-unity Lewis number or preferential diffusion effects [13]. Non-unity Lewis number effects are due to local energy imbalances brought about by differences between the relative diffusion rates of heat (by thermal diffusion) and chemical energy (by mass diffusion). Preferential diffusion is due to differences in the mass diffusivities of the reactant constituents, leading to local variations in equivalence ratio.

Before discussing the impact of these fuel effects, it is important to discuss some aspects of the turbulent flame speed. As detailed in two recent reviews [14-15] and through the International Workshop on Premixed Flames [16], there are multiple useful definitions for S_T that are relevant for different combustion issues (e.g., flashback versus heat release per volume). Four definitions of S_T have been proposed: local displacement speed, $S_{T,LD}$, global displacement speed, $S_{T,GD}$, local consumption speed, $S_{T,LC}$, and global consumption speed, $S_{T,GC}$ [14-16]. This paper focuses on $S_{T,GC}$ measurements, defined as:

$$S_{T,GC} = \frac{\dot{m}_R}{\rho_R \overline{A}_{\langle c \rangle}} \quad (1)$$

where $\dot{m}_R$, ρ_R and $\overline{A}_{<c>}$ denote reactant mass flow rate, reactant density and mean flame area corresponding to some prescribed $<c>$ contour.

This paper extends several prior studies by the authors on $S_{T,GC}$ characteristics of H_2/CO blends [17-18]. The key new contribution of this work is correlation of these data using a physics-based model incorporating the leading points concept. Leading points are defined as the positively curved points on the flame that propagate out farthest into the flame [10, 19-20]. The leading point is established where the local flame speed is greater than the local flow velocity. Due to this kinematic imbalance, the flame propagates out into this point. For negative Markstein length mixtures, the burning rate of this positively curved leading point increases [13]. Because the turbulent burning velocity is controlled by the leading point characteristics [20], the ensemble averaged laminar burning rate of this leading point turns out to be a very significant turbulent flame property.

EXPERIMENTAL APPROACH AND FACILITY

This study focuses upon measurements of $S_{T,GC}$ using a turbulent Bunsen flame, an $S_{T,GC}$ measurement approach recommended by Gouldin and Cheng [16]. This configuration was used because of the wide variety of available data in similar geometries for benchmarking and comparisons [21].

This experimental facility has been detailed extensively in the previous work [17-18] but a short description is provided. A schematic of the system is shown in Figure 1. The burner is a smoothly contoured nozzle with high contraction ratio to inhibit boundary layer growth and to achieve a top hat exit velocity profile. Measurements were taken using burners with 12 and 20 mm exit diameters. An annular sintered plate is placed around the burner outlet to hold a premixed, methane-air pilot flame, to stabilize the main flame. The total mass flow rate of the pilot does not exceed 5% of the main flow rate to ensure minimal impact of the pilot on the main flame.

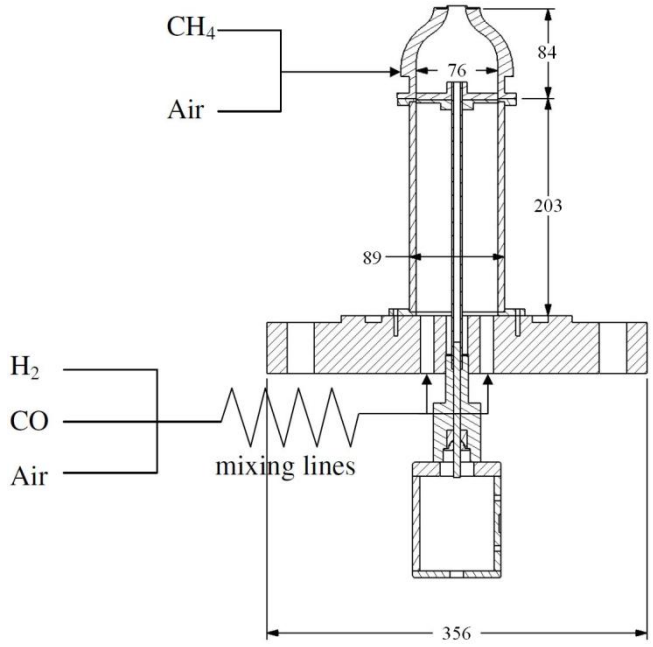

Figure 1: Schematic of the experimental facility. Dimensions in mm.

The turbulence intensity is varied independently of the mean flow velocity using a remotely controlled turbulence

generator. This turbulence generator assembly consists of milled slots in a thin plate that cause flow separation and vorticity generation as the flow passes through them. These vortical structures impinge on the inclined wall of the converging section of the nozzle, breaking them down into finer turbulent eddies [22].

Complete details on the features of the variable turbulence generator as well as the velocity characterization studies conducted using LDV and PIV can be found in Venkateswaran *et al.* [17] and Marshall *et al.* [18].

Image Analysis

Global consumption speeds were calculated using Eq. (1), whose key measurement input is progress variable surface area, $\bar{A}_{<c>}$. Digital images of the flame emission are captured with a 16-bit intensified charge-coupled device (ICCD) camera. Line of sight images of the flame were obtained over 5 seconds and time-averaged. Note that other potential Bunsen flame $S_{T,GC}$ measurement approaches include Mie scattering [21, 23] or OH-PLIF [24] measurements for flame characterization. The resulting progress variable contours (described below) are equivalent for the two methods, assuming that the OH-PLIF or Mie interface surface is equivalent to the chemiluminescence flamelet surface [25]. This line-of-sight approach was used here, however, because the OH-PLIF or Mie scattering technique does not capture flame surface density in the out-of-plane direction and, as such, significantly underestimates it. The spatial distribution of heat release is fully captured by a line of sight measurement.

To estimate the time-averaged flame brush location from the line-of-sight images, a three-point Abel deconvolution scheme [26] was used. The axial distribution of the centerline intensity is then fit to a Gaussian curve, from which the location of the maximum intensity is identified. This point is associated with the most probable location of the flame, and defined as the $<c>$ = 0.5 progress variable contour. The estimated uncertainty in identifying this point is 1-2%. Straight lines are then drawn from this point to the two flame anchoring points and rotated about the line of symmetry to generate a cone; i.e., the "angle method" [9, 21, 27]. The overall uncertainty in the estimated $S_{T,GC}$ value is estimated to be 3%.

RESULTS AND DISCUSSION

Two basic sets of tests were performed. Measurements of $S_{T,GC}$ were obtained as a function of $u'_{rms}/S_{L,0}$ for 12 and 20 mm burner diameters at mean flow velocities from 4-50 m/s and volumetric H_2/CO ratios from 30/70 – 90/10, keeping $S_{L,0}$ and reactant temperature fixed at 34 cm/s and 300 K respectively. $S_{L,0}$ was kept nominally constant by adjusting the stoichiometry at each H_2/CO ratio. Additionally, a CH_4/air data set was obtained at the same $S_{L,0}$ (ϕ = 0.9). $S_{L,0}$ estimates were determined using the CHEMKIN software with the Davis H_2/CO mechanism for H_2/CO mixtures [28] and GRI 3.0 for CH_4/air [29]. Symbol type and color scheme are summarized in Table 1 and Table 2.

Table 1: Legend used for the constant $S_{L,0}$ data set for the 20 mm burner

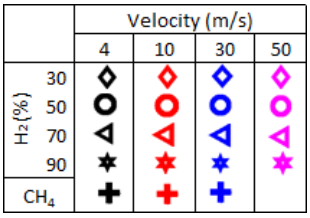

Table 2: Legend used for the constant $S_{L,0}$ data set for the 12 mm burner

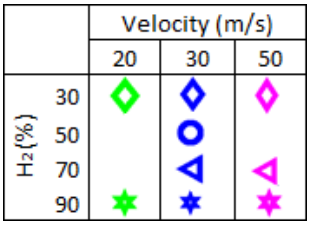

The second set of tests was performed by sweeping the equivalence ratio at constant H_2/CO ratio values of 30/70 and 60/40 with the 20 mm burner. The symbol type and color scheme used for this data set are summarized in Table 3.

Table 3: Legend for constant H_2 content equivalence ratio sweeps data for the 20 mm burner

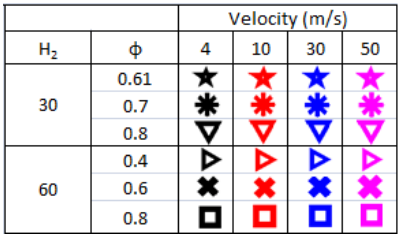

The parameter ranges explored in this study are summarized in Table 4. Figure 2 summarizes where the measured data is located on a Borghi diagram [30], showing the location of both 12 and 20 mm burner diameter data sets.

Table 4: Investigated parameter space

	Constant $S_{L,0}$				ϕ Sweep					CH_4
U_0 (m/s)	4, 10, 30, 50									4, 10, 30
H_2 (%)	30	50	70	90	30		60			0
ϕ	0.61	0.55	0.51	0.48	0.7	0.8	0.4	0.6	0.8	0.9
$S_{L,0}$ (m/s)	0.34				0.48	0.59	0.15	0.51	0.9	0.34

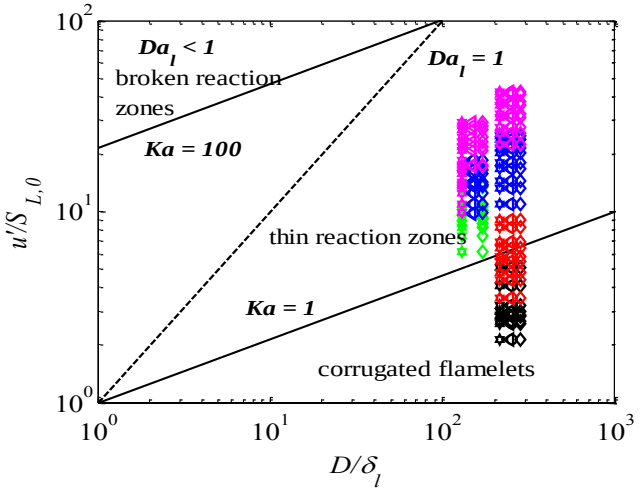

Figure 2: Borghi diagram showing location of constant $S_{L,0}$ study data points for 12 and 20 mm burners.

Flame speed stretch sensitivities were also calculated using an opposed flow calculation of two premixed flames with a nozzle separation distance of 20 mm, using the OPPDIF module in CHEMKIN. From these calculations various properties of the strained values were extracted. The S_L value reported here is defined as the minimum velocity just ahead of the reaction zone, as suggested by Wu and Law [31]. The Markstein length, l_M, was determined from the slope of the linear fit in the low strain regime of the κ vs. S_L curve. Extinction strain rates, κ_{ext} were calculated using an arc length continuation method [32]. An example set of calculations for the constant $S_{L,0}$ mixtures are shown in Figure 3, showing the convergence of the different mixtures toward the same $S_{L,0}$ at κ = 0. However, they clearly have different stretch sensitivities as quantified by the Markstein length and extinction strain rates. These stretch sensitivities are used later in the flame speed correlation section to facilitate analysis of these data.

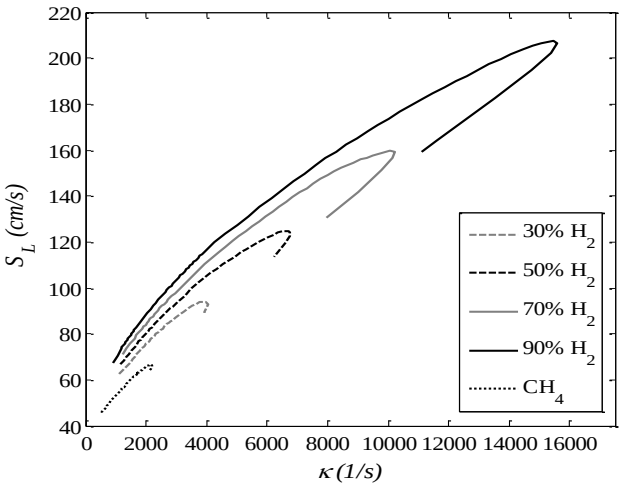

Figure 3: Stretch sensitivity calculations of constant $S_{L,0}$ mixtures (see Table 4 for ϕ values)

H_2/CO Sweeps at Constant $S_{L,0}$

This section presents data for various H_2/CO ratios at nominally constant $S_{L,0}$. Figure 4 and Figure 5 plot $S_{T,GC}/S_{L,0}$ for H_2/CO mixtures of 30/70, 50/50, 70/30, and 90/10 at mean flow velocities of 4, 10, 30, and 50 m/s for the 20 mm burner. These two graphs plot the same data on a linear (Figure 4) and log (Figure 5) scale. As expected, $S_{T,GC}$ increases monotonically with turbulence intensity, for a given fuel composition. The main observation from this data is the monotonically increasing value of $S_{T,GC}$ with H_2 levels. For example, at U_0 = 30 m/s and $u'_{rms}/S_{L,0}$ = 25, $S_{T,GC}/S_{L,0}$ has a value of 8 for CH_4, of 14 for the 30/70 H_2/CO mix and 22 for the 90/10 H_2/CO mix. Moreover, the data indicate that these "fuel effects" persist even at very high turbulence intensities. Note also the significant similarities between each fixed mean flow velocity, U_0, group as fuel composition is varied. It appears that the same curve is shifted vertically to higher $S_{T,GC}$ values as H_2 fraction is increased.

Also included on these graphs for reference are several measured or predicted S_T correlations (discussed in detail in Venkateswaran *et al.* [17]). Some caution should be exercised in comparing these with the data, because of the definition dependence of S_T and u'_{rms} noted earlier. Although many of these are local consumption speed based correlations, they do reasonably bracket the results.

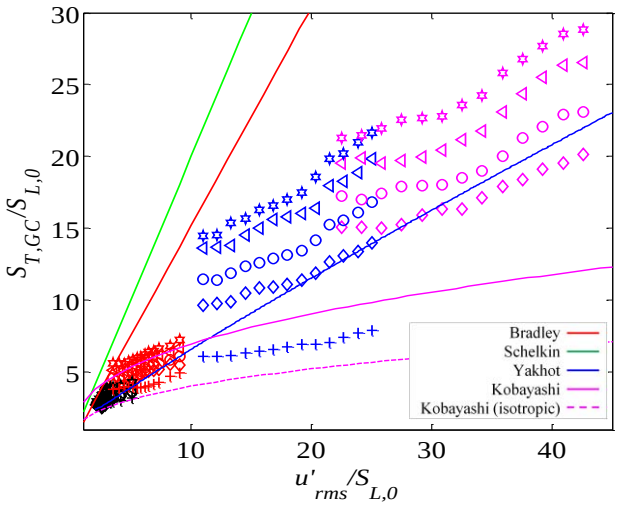

Figure 4: Linear plot of dependence of turbulent flame speed, $S_{T,GC}$, upon turbulence intensity, u'_{rms} , normalized by $S_{L,0}$ at various mean flow velocities and H_2/CO ratios for the 20 mm burner. (See Table 1 for legend of mixture conditions and flow velocities)

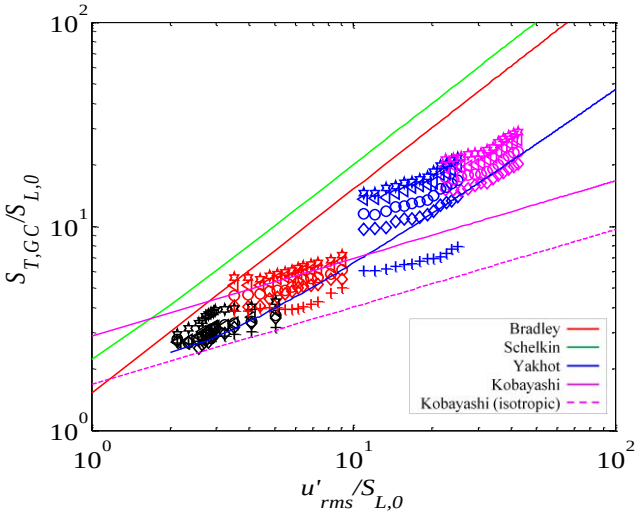

Figure 5: Log-log plot of variations of turbulent flame speed, $S_{T,GC}$, with turbulence intensity, u'_{rms} , normalized by $S_{L,0}$ at various mean flow velocities and H_2/CO ratios for the 20 mm burner. (See Table 1 for legend of mixture conditions and flow velocities)

The data for the 12 mm burner at various H_2/CO ratios at nominally constant $S_{L,0}$ are summarized in Figure 6, which plots $S_{T,GC}/S_{L,0}$ for H_2/CO blends at mean flow velocities of 20, 30, and 50 m/s.

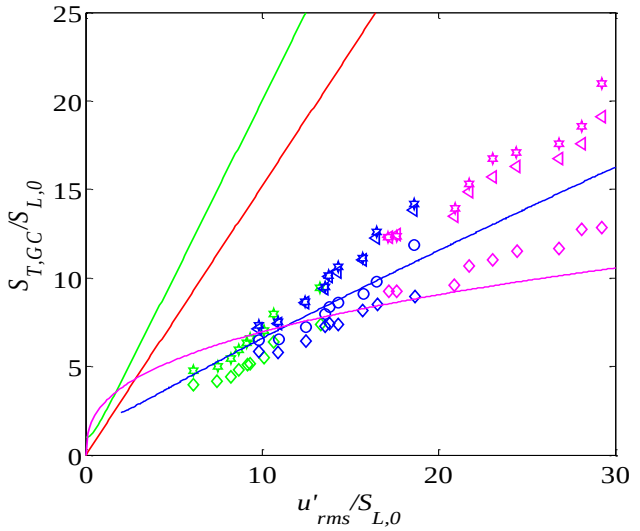

Figure 6: Variations of turbulent flame speed, $S_{T,GC}$, with turbulence intensity, u'_{rms}, normalized by $S_{L,0}$ at various mean flow velocities and H_2/CO ratios for the 12 mm burner. (See Table 2 for legend of mixture conditions and flow velocities)

Note that larger average consumption speeds are seen with the larger burner diameter, at a given fuel composition, turbulence intensity, and mean flow velocity. These differences are about 50% for 50 m/s and 60% for 30 m/s. This shows the well known length scale sensitivity of the turbulent flame speed [6].

Although not the primary focus of this study, the mean flow dependencies at a given fuel composition are worthy of mention. First, these data clearly show the well known dependence of $S_{T,GC}$ upon U_0, a fact highlighted in Refs. [7, 14]. Each velocity result appears to lie on its own curve, which is parallel to the lower velocity case, but does not intersect it at the same turbulence intensity. This is particularly evident for $u'_{rms}/S_{L,0} = 10$ at $U_0 = 10$ and 30 m/s, and $u'_{rms}/S_{L,0} = 5$ for $U_0 = 4$ and 10 m/s where $S_{T,GC}/S_{L,0}$ differs by 100% and 36% for the 90% H_2 mixture, respectively. This mean flow dependence is less obvious at the $u'_{rms}/S_{L,0} = 23$ case between the $U_0 = 30$ and 50 m/s cases, presumably because the fractional variation in U_0 is much smaller in this case.

Equivalence Ratio Sweeps

Equivalence ratio sweeps were also performed at fixed H_2 contents of 30% and 60% for three equivalence ratios using the 20 mm burner diameter. The symbols used for Figure 7 and Figure 8 are presented in Table 3. Figure 7 show the results for a 60% H_2 mixture at ϕ = 0.4, 0.6, 0.8 for mean flow velocities of 4, 10, 30, and 50 m/s. Note that $S_{L,0}$ is not held nominally constant for these data, as it was in the prior section.

As in Figure 4 through Figure 6, the S_T correlations have also been plotted. From Figure 7 it is seen that the data generally fall within the band formed by the Bradley and Yakhot correlations. Furthermore, the slope of the data seems to agree quite well with Kobayashi's correlation, particularly at the low to intermediate $u'_{rms}/S_{L,0}$ ranges.

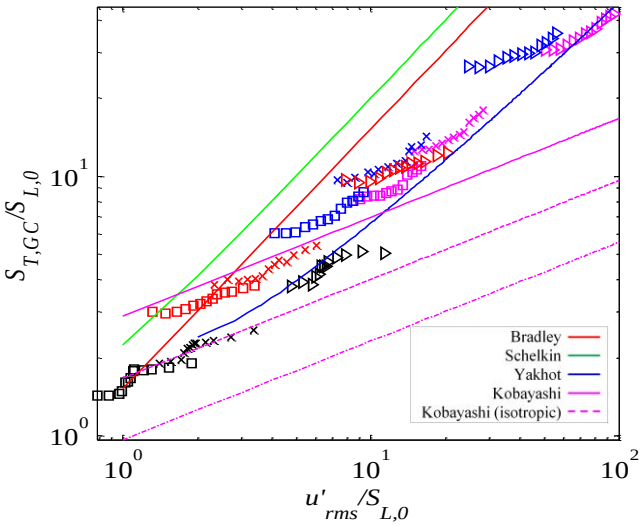

Figure 7: Variations of turbulent flame speed, $S_{T,GC}$, with turbulence intensity, u'_{rms}, normalized by $S_{L,0}$ for various mean flow velocities and equivalence ratios at a fixed H_2 content of 60%. (See Table 3 for legend of mixture conditions and flow velocities)

Figure 8 shows the results for a 30% H_2 mixture at ϕ = 0.61, 0.7, 0.8 for mean flow velocities of 4, 10, 30, and 50 m/s. Similar conclusions can be reached from this data as discussed above.

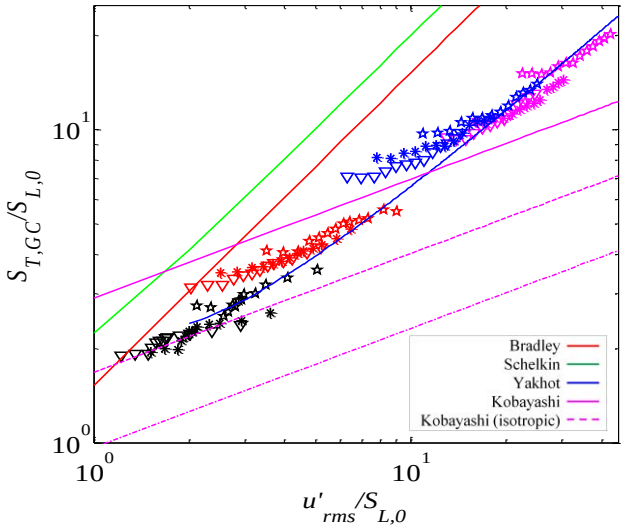

Figure 8: Variations of turbulent flame speed, $S_{T,GC}$, with turbulence intensity, u'_{rms}, normalized by $S_{L,0}$ at various mean flow velocities and equivalence ratios at a fixed H_2 content of 30%. (See Table 3 for legend of mixture conditions and flow velocities)

Again from Figure 8, it can be seen that the data generally fall within the band created by the Bradley and Yakhot correlations. Furthermore, since the $u'_{rms}/S_{L,0}$ range investigated with the 30/70 H_2/CO mixture is smaller, it is easier to see that the Yakhot correlation is a close match.

ANALYSIS OF FLAME SPEED DATA

These data are consistent with prior studies showing that stretch sensitivity of the reactants has an important impact on the turbulent flame speed [5, 14]. This point is shown in Figure 9, which plots the dependence of $S_{T,GC}/S_{L,0}$ of the data reported in this paper upon calculated Markstein length of the reactants, l_M (see Figure 3), at two different turbulence intensities for the constant $S_{L,0}$ studies. The point located at l_M = -0.02 cm for $u'_{rms}/S_{L,0}$ = 20 corresponds to the methane-air mixture at ϕ = 0.9. Note the monotonically increasing value of $S_{T,GC}$ with $|l_M|$. Also, the difference in flame speeds between low and high H_2 flames for the H_2/CO blends and the CH_4/air and H_2/CO/air flames is significant, being as large as two and three, respectively.

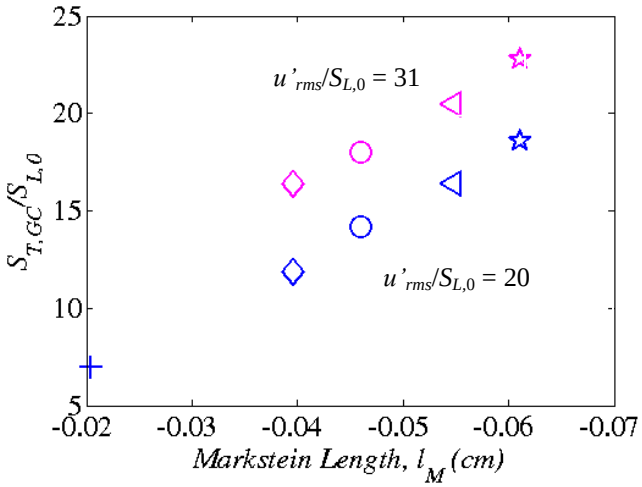

Figure 9: Dependence of measured $S_{T,GC}/S_{L,0}$ upon calculated Markstein length, l_M, for $u'_{rms}/S_{L,0}$ = 20 and 31 at $S_{L,0}$ = 0.34 m/s.

A common approach for scaling turbulent flame speeds is to use the consumption based definition [14]:

$$S_T = \frac{\langle S_L A \rangle}{A_0} \tag{2}$$

Or, by introducing the stretch factor, I_0 [33-34]:

$$S_T = \frac{S_{L,0} \langle I_0 A \rangle}{A_0} \tag{3}$$

For stretch insensitive flames, the I_0 factor equals unity, leading to the classical S_T scaling described by Damköhler [35]. For stretch sensitive flames, one is left with the function $\langle I_0 A \rangle$, which requires understanding the correlation between local flame speed and flame area. Assuming that these functions are uncorrelated, i.e., that $\langle I_0 A \rangle = \langle I_0 \rangle \langle A \rangle$ leads to the erroneous prediction that the mixture's stretch sensitivity should not influence S_T [36]. This prediction follows from measurements and computations which show that the flame curvature PDF is roughly symmetric about κ = 0 [37-40], implying that regions of enhanced and diminished local consumption rate should roughly cancel and, thus, that $\langle I_0 \rangle \approx 1$. Hydrodynamic strain, which is not symmetric about κ = 0 [39-41] does introduce a non-unity $\langle I_0 \rangle$ value, but it seems unlikely that this effect is significant enough to explain the appreciable fuel effects reported here and in the literature.

However, it can easily be seen that assuming uncorrelated A and I_0 passes over key physics: in particular, there are implicit I_0 effects in the $\langle A \rangle$ term because the local flame speed and area are highly correlated. For example, if the positively curved leading point of the flame has a higher local flame speed, it will propagate at a faster speed into the unburned reactants, increasing flame area accordingly. In the same way, the slower, negatively curved trailing point of the flame will lag backwards, also increasing flame area.

Given the implicit presence of I_0 in the $\langle A \rangle$ term, modeling approaches based upon leading points concepts [5, 10, 20] may be more useful for explicitly bringing out stretch sensitivity effects. The leading points are roughly defined as the necessarily positively curved points on the turbulent flame front that propagate farthest into the reactants. It has been argued that the propagation speed of these points with respect to the average flow velocity control the overall turbulent flame speed [20]. As a result, fuel/air mixtures with negative Markstein numbers will have enhanced laminar flame speeds at the positively curved leading points, resulting in larger displacement speeds.

This basic leading points argument can be readily understood from the simple model problem of a flat flame propagating into a spatially varying velocity field, as depicted in Figure 10.

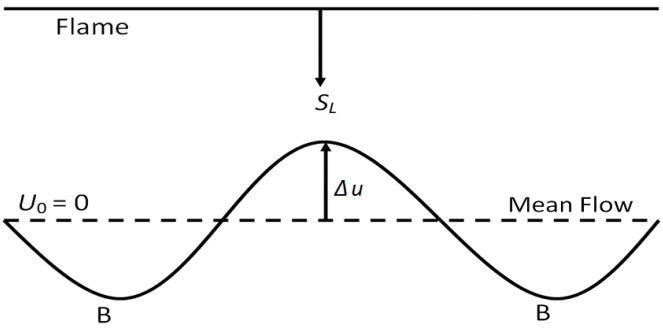

Figure 10: Model problem of a flat flame propagating into a spatially varying flow field with zero mean velocity.

If we assume that S_L remains constant, then it is seen that the portion of the flame at the lowest velocity point propagates out the fastest. In the lab-fixed coordinate system, the flame at Point B moves at a speed of $S_L + (\Delta u)_{LP}$, where the subscript "*LP*" denotes the leading point. Moreover, it can easily be shown by a front tracking computation that, after an initial transient, the entire front reaches a stationary shape and propagation speed which has the same value; i.e., $S_D = S_L + (\Delta u)_{LP}$. As such, the overall displacement speed is controlled by the leading points of the flame that propagate into the lowest velocity regions ahead of the flame. Note also that the flame area would increase as well, but this is an *effect* of the higher displacement speed, not the *cause*.

In reality, the positively curved leading point of the flame will have an altered flame speed, $(S_L)_{LP} = S_{L,0} + \left(S_L'\right)_{LP}$, where $\left(S_L'\right)_{LP}$ is the modification of the un-stretched laminar flame speed at the leading point, because of the mixtures nonzero Markstein length. If the mixture has a negative Markstein number, then the flame speed at this point will further increase, causing an increase in curvature, further increasing the local flame speed. This is analogous to the processes causing the thermo-diffusive instability in premixed flames [13]. As a result, the above expression can be modified to take into account the flame speed augmentation:

$$S_D = \left(S_L\right)_{LP} + \left(\Delta u\right)_{LP} \tag{4}$$

The key difference to note from this scaling approach relative to Eq. (3) is that this focuses on a local flame characteristic – namely the positively curved leading point – as opposed to the global average, $\langle I_0 A \rangle$, which obscures the stretch effect.

The key problem lies in scaling $\left(S_L'\right)_{LP}$. If the positively curved leading point is weakly stretched, then $\left(S_L'\right)_{LP} \sim l_M \kappa_{LP}$. This switches the problem to scaling the strain statistics conditioned on the leading point of the flame, κ_{LP}, an important fundamental problem in turbulent combustion; see Lipatnikov and Chomiak [5] for discussion. However, the value of $(S_L)_{LP}$ is bounded by some $S_{L,max}$ value; e.g., for an opposed flow flame, $S_{L,max}$ can be directly extracted from the simulations shown in Figure 3. Thus, note that $S_{L,max} > (S_L)_{LP} > S_{L,0}$. For example, this leads to the following inequality for the 30% H_2 blend: 95 cm/s > $(S_L)_{LP}$ > 34 cm/s. Substituting this $S_{L,max}$ value in for $(S_L)_{LP}$ and writing $(\Delta u)_{LP}$ as u'_{LP}, leads to the following:

$$\frac{S_D}{S_{L,\max}} \le 1 + \frac{u'_{LP}}{S_{L,\max}} \tag{5}$$

Note that this is nearly identical to Damköhler's classical result [35] where S_L has been replaced by $S_{L,max}$ and u' by u'_{LP}.

This inequality can be replaced by an equality in certain situations. Since the mixtures investigated are thermo-diffusively unstable, $S_{L,0}$ is a 'repelling' point since a positively curved perturbation on a flat flame will grow with increasing curvature and correspondingly increasing flame speeds as shown in Figure 3. In fact, as is shown rigorously in the appendix, $S_{L,max}$ is a steady-state 'attracting' point for positively curved wrinkles. As such, if the turbulent eddies evolve over a time scale that is slow relative to that required for the leading points to be attracted to the $S_{L,max}$ point, then Equation (5) can be replaced by:

$$\frac{S_D}{S_{L,\max}} = 1 + \frac{u'_{LP}}{S_{L,\max}} \qquad (6)$$

On the basis of the scaling derived above, all the $S_{T,GC}$ data presented above are replotted using the $S_{L,max}$ normalization. Because of the mean flow dependencies noted earlier, we plot this data first at fixed flow velocities

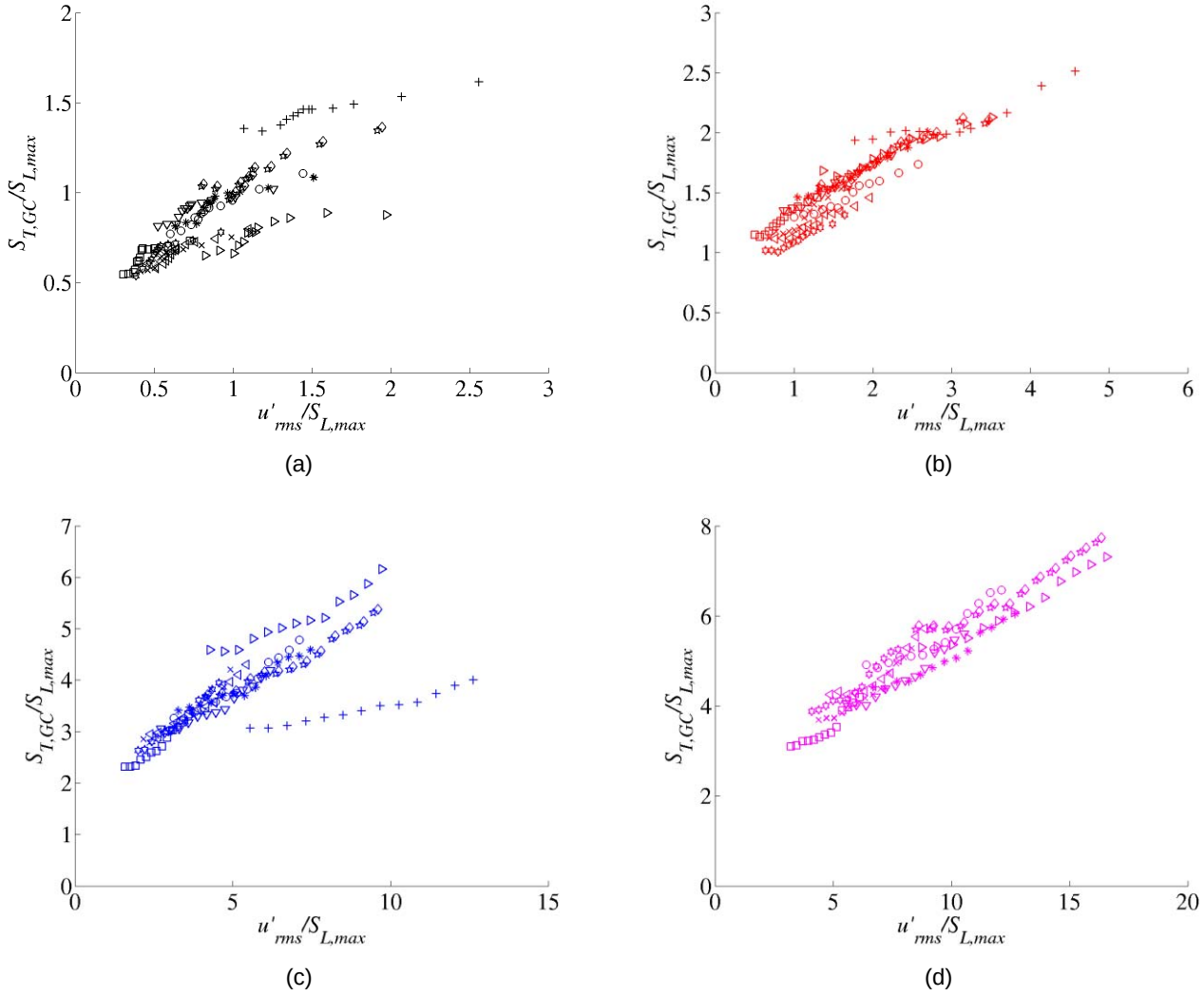

Figure 11: Variations of the turbulent flame speed, $S_{T,GC}$, with turbulence intensity u'_{rms} normalized by $S_{L,max}$ for 20 mm burner grouped by mean flow velocities (a) 4 m/s (b) 10 m (c) 30 m/s (d) 50 m/s. (See Table 1 and Table 3 for legend)

Figure 11 shows that the data collapses generally well across all the mean flow velocities. There is some scatter in the 4 m/s data that largely disappears at the higher flow velocities. Also, note that the 30 m/s CH_4/air data does not collapse with the H_2/CO data set while it collapses at 10 m/s and 4 m/s.

Figure 12 plots the entire 20 mm burner data set, which contains both the constant $S_{L,0}$ studies and the equivalence ratio sweep studies, while Figure 13 displays the renormalized 12 mm burner data.

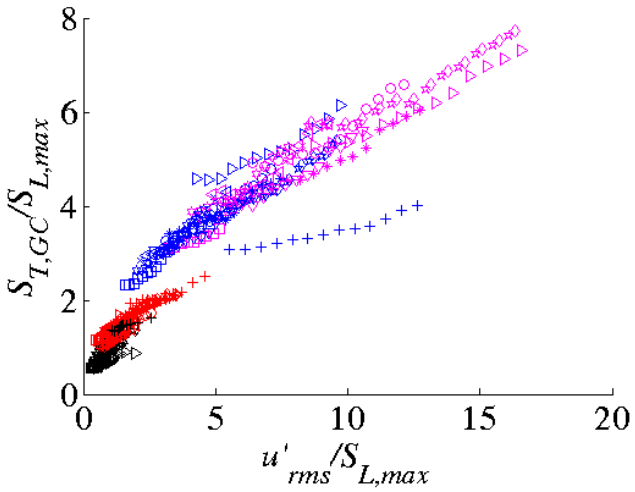

Figure 12: $S_{L,max}$ normalized $S_{T,GC}$ data for the 20 mm burner (see Table 1 and Table 3 for legend)

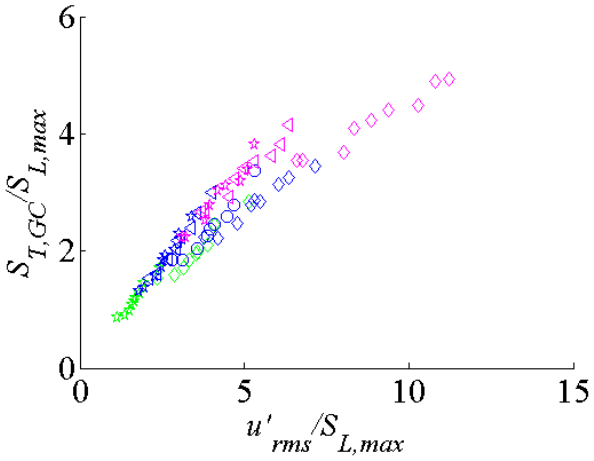

Figure 13: $S_{L,max}$ normalized $S_{T,GC}$ data for the 12 mm burner for constant $S_{L,0}$ studies (see Table 2 for legend)

From Figure 12 and Figure 13 it is clear that both data sets collapse very well, with the exception of the 30 m/s CH_4 data. In fact for the 20 mm constant $S_{L,0}$ data set, the variation in the normalized turbulent flame speed values for the 30/70 to 90/10 reduced from 50% to about 10% (for the 50 m/s case) between Figure 4 and Figure 12. Larger disparities (about 50% at $u'_{rms}/S_{L,max}$ = 12.5) are seen between the H_2/CO data and CH_4 data. This scatter and some caveats are discussed further in the following paragraphs.

First, some scatter is inevitable as the κ_{ext} and $S_{L,max}$ value are not constants for a given mixture but depends upon the strain profile the flame is subjected to [42]. For example, repeating these calculations using nozzle separation distances ranging from 10 to 40 mm causes variations in $S_{L,max}$ of 5% for the 30/70 H_2/CO mixture. Moreover, this $S_{L,max}$ value is a function of the experimental configuration – in particular, the sensitivity of strained and curved flames to high levels of stretch are different. Presumably, the $S_{L,max}$ at the leading point of the turbulent flame brush would be related to the strain rate associated with the highly curved leading edge, whose radius of curvature is bounded by the flame thickness.

Second, the local burning velocity at the leading point, $(S_L)_{LP}$ is not identically equal to $S_{L,max}$; rather, $S_{L,max}$ is simply an upper bound of an inequality as discussed earlier. As discussed early, only in the quasi-steady turbulence limit can this inequality be replaced by equality.

Third, from the derivation of the scaling, it is evident that this scaling may be more suitable for a local displacement turbulent flame speed definition.

Finally, note that the $S_{T,GC}$ data reported here by virtue of Equation (1) necessarily average over potentially significant variations in local flame speeds whereas the scaling shown in Equation (5) is essentially valid at a single point on the instantaneous flame front. As a result, adjustments to suitably average over a spatially developing flow field and flame brush are required. Nonetheless, the very good collapse of the large data set obtained here provides strong evidence for the basic validity of the scaling argument shown in Equation (5). Note that this argument will need revisiting for $l_M > 0$ flames, where the attracting point argument discussed above requires modification.

CONCLUDING REMARKS

The data presented in this paper show the strong dependence of the turbulent consumption speed upon fuel consumption, even at large turbulence intensities. It is believed that these observed fuel effects are due to the stretch sensitivity of the reactant mixture, which has a strong effect at the positively curved leading points on the turbulent flame front for negative Markstein length mixtures. The leading points concept was used to develop a new scaling law which was very similar to Damkohler's scaling of the turbulent flame speed, except that $S_{L,max}$ arises as the normalization parameter, instead of S_L. We showed that the scaling law does a reasonable job of collapsing the data set. However, additional work is needed to develop better scaling rules for the leading point strain statistics, as well as to develop averaging procedures to capture spatial variations in the turbulent consumption speed that are present in any global consumption speed.

ACKNOWLEDGEMENTS

This research was partially supported by University Turbine Systems Research program, Mark Freeman, contract monitor, under contract DE-FC21-92MC29061, by Siemens Energy through a subcontract with DOE prime contract DE-FC26-05NT42644, Dr. Scott Martin contract monitor, and by University of California-Irvine through a subcontract with the California Energy Commission. The authors gratefully acknowledge Mr. Juan Camilo Pedroza for his assistance in

assembling the experimental facility and data collection, Ms. Yikai Chen for performing the stretch sensitivity calculations, and Reaction Design for making available the new release 15091 of CHEMKIN-PRO©.

NOMENCLATURE

A	Instant flame area
A_0	Mean flame area
$\overline{A}_{<c>}$	Mean flame area associated with given <c> contour
<c>	Progress variable contour
G	Level-set function
g	Slope of flame location
I_0	Stretch factor
κ	Stretch rate
κ_{LP}	Leading point stretch rate
l_M	Markstein length
P	Pressure
P_0	Standard pressure
Re_D	Reynolds number
S_D	Leading point displacement speed
S_L	Stretched laminar flame speed
$S_{L,0}$	Un-stretched laminar flame speed
$(S_L')_{LP}$	Modification of laminar flame speed at leading point
$(S_L)_{LP}$	Leading point laminar flame speed
$S_{L,max}$	Maximum stretched laminar flame speed
S_T	Turbulent flame speed
$S_{T,GC}$	Global turbulent consumption speed
$S_{T,GD}$	Global turbulent displacement speed
$S_{T,LC}$	Local turbulent consumption speed
$S_{T,LD}$	Local turbulent displacement speed
$(\Delta u)_{LP}$	Leading point velocity deficit
U	Instantaneous axial velocity
U_0	Mean axial velocity
V	Instantaneous transverse velocity
l_{int}	Integral length scale
$\dot{m}_R$	Reactant mass flow rate
u'_{rms}	Root mean square turbulence fluctuations
u'_{LP}	Leading point turbulence intensity
ρ_R	Reactant density
ξ	Flame position
ϕ	Equivalence ratio

APPENDIX

As discussed earlier, $S_{L,max}$ is a steady-state 'attracting' point for positively curved wrinkles. This can be shown formally by considering the following level set equation describing the flame's spatio-temporal dynamics:

$$\frac{\partial G}{\partial t} + \vec{u} \cdot \vec{\nabla} G = S_L \left| \vec{\nabla} G \right| \tag{A1}$$

This is a suitable model for the flame's dynamics, as Figure 2 shows that the data falls primarily in the corrugated flamelets and thin reaction zone regimes. This equation can be treated analytically in the low turbulence intensity limit, where the flame position is a single-valued function of some coordinate $G = y - \xi(x, t)$, as shown in Figure 14.

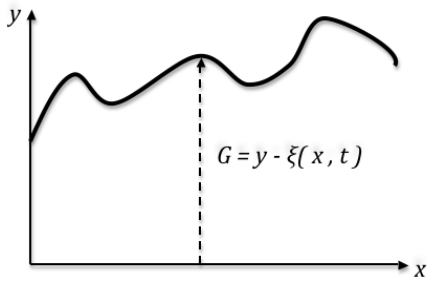

Figure 14: Coordinate system defining the instantaneous flame location, $\xi(x, t)$.

Writing the stretch sensitive flame speed as $S_L = S_{L,0}[1 + f(\kappa)]$, we obtain:

$$-\frac{\partial \xi}{\partial t} - U\frac{\partial \xi}{\partial x} + V = S_{L,0}\left[1 + f(\kappa)\right]\left[1 + \left(\frac{\partial \xi}{\partial x}\right)^2\right]^{1/2} \tag{A2}$$

Differentiating this expression with respect to x, and substituting g for $\partial\xi/\partial x$:

$$\begin{aligned} -\frac{\partial g}{\partial t} - \frac{\partial}{\partial x}(Ug) + \frac{\partial V}{\partial x} &= S_{L,0}\left(1+g^2\right)^{1/2}\frac{\partial f}{\partial \kappa}\frac{\partial \kappa}{\partial x} \\ &+ S_{L,0}\left[1 + f(\kappa)\right]\frac{g}{\left(1+g^2\right)^{1/2}}\frac{\partial g}{\partial x} \end{aligned} \tag{A3}$$

A necessary condition for leading points, located at the points, x_{LP}, is that $g(x_{LP}, t) = 0$ and $\partial g(x_{LP}, t)/\partial x < 0$. We can determine the asymptotic tendencies of these leading points in a quiescent medium by taking the steady state limit of this equation by setting $\partial g/\partial t = 0$ and $U = V = 0$. Furthermore, by explicitly writing the curvature induced strain, κ, as $\frac{\partial g/\partial x}{\left(1+g^2\right)^{3/2}}$, Equation (A3) can then be expressed as:

$$0 = S_{L,0}\left(1+g_{ss}^2\right)^{1/2}\frac{\partial f}{\partial \kappa}\left[\frac{\partial^2 g_{ss}}{\partial x^2}\left(1+g_{ss}^2\right)^{-3/2} - 3g_{ss}\left(1+g_{ss}^2\right)^{-5/2}\left(\frac{\partial g_{ss}}{\partial x}\right)^2\right] + S_{L,0}\left[1+f(\kappa)\right]\frac{g_{ss}}{\left(1+g_{ss}^2\right)^{1/2}}\frac{\partial g_{ss}}{\partial x} \tag{A4}$$

Setting $g_{ss} = 0$ shows that the following necessary condition is satisfied at the leading point:

$$\frac{\partial f}{\partial \kappa}\frac{\partial^2 g_{ss}}{\partial x^2} = 0 \tag{A5}$$

Equation (A5) shows that the steady-state leading points must occur where $\partial f/\partial \kappa = 0$, which coincides with the location of $S_L = S_{L,max}$. Physical arguments can also be used to show that this is a stable attracting point if $\partial^2 f/\partial \kappa^2 < 0$, and that $\partial g/\partial x < 0$ at this $\partial f/\partial \kappa = 0$ point.

The above analysis clearly shows that equating $(S_L)_{LP}$ with $S_{L,max}$ is appropriate in the "quasi-steady" limit of slow turbulent fluctuations. In reality, the leading points continuously evolve in time, as the character of the turbulent fluctuations change, causing points to move back and forth, with the leading points at a given instant approximately corresponding to the points of local minimum in velocity. Further analysis is needed to understand these unsteady effects.

REFERENCES

[1] Richards, G. A., and Casleton, K. H., 2009, Synthesis Gas Combustion: Fundamentals and Applications, CRC Press, Gasification Technology to Produce Synthesis Gas.

[2] Lieuwen, T., Mcdonell, V., Petersen, E., Santavicca, D., 2008, "Fuel Flexibility Influences on Premixed Combustor Blowout, Flashback, Autoignition, and Stability," Journal of Engineering for Gas Turbines and Power, 130(pp. 011506.

[3] Lieuwen, T. C., Yang, V., 2005, "Combustion Instabilities in Gas Turbine Engines (Operational Experience, Fundamental Mechanisms and Modeling)," Progress in Astronautics and Aeronautics, pp.

[4] Figura, L., Lee, J. G., Quay, B. D., and Santavicca, D. A., 2007, "The Effects of Fuel Composition on Flame Structure and Combustion Dynamics in a Lean Premixed Combustor," ASME Conference Proceedings, 2007(47918), pp. 181-187.

[5] Lipatnikov, A. N., and Chomiak, J., 2005, "Molecular Transport Effects on Turbulent Flame Propagation and Structure," Progress in Energy and Combustion Science, 31(1), pp. 1-73.

[6] Lipatnikov, A. N., and Chomiak, J., 2002, "Turbulent Flame Speed and Thickness: Phenomenology, Evaluation, and Application in Multi-Dimensional Simulations," Progress in Energy and Combustion Science, 28(1), pp. 1-74.

[7] Filatyev, S. A., Driscoll, J. F., Carter, C. D., and Donbar, J. M., 2005, "Measured Properties of Turbulent Premixed Flames for Model Assessment, Including Burning Velocities, Stretch Rates, and Surface Densities," Combustion and Flame, 141(pp. 1-21.

[8] Ballal, D. R., and Lefebvre, A. H., 1973, "Turbulence Effects on Enclosed Flames," Acta Astronautica, 1(3-4), pp. 471-483.

[9] Ballal, D., and Lefebvre, A., 1975, "The Structure and Propagation of Turbulent Flames," Proceedings of the Royal Society of London. Series A, Mathematical and Physical Sciences, 344(1637), pp. 217-234.

[10] Kuznetsov, V. R., and Sabel'nikov, V. A., 1986, Turbulence and Combustion, Hemisphere Publishing Corporation, Moscow, Turbulent Combustion of a Homogenous Mixture.

[11] Nakahara, M., and Kido, H., 2008, "Study on the Turbulent Burning Velocity of Hydrogen Mixtures Including Hydrocarbons," AIAA Journal, 46(7), pp. 1569-1575.

[12] Kido, H., Nakahara, M., Nakashima, K., and Hashimoto, J., 2002, "Influence of Local Flame Displacement Velocity on Turbulent Burning Velocity," Proceedings of the Combustion Institute, 29(2), pp. 1855-1861.

[13] Law, C. K., 2006, *Combustion Physics*, Cambridge University Press, New York.

[14] Driscoll, J. F., 2008, "Turbulent Premixed Combustion: Flamelet Structure and Its Effect on Turbulent Burning Velocities," Progress in Energy and Combustion Science, 34(1), pp. 91-134.

[15] Cheng, R. K., 2009, Synthesis Gas Combustion: Fundamentals and Applications, CRC Press, Turbulent Combustion Properties of Premixed Syngas.

[16] Gouldin, F., and Cheng, R. K., International Workshop on Premixed Turbulent Flames, http://eetd.lbl.gov/aet/combustion/workshop/workshop.html

[17] Venkateswaran, P., Marshall, A. D., Noble, D. R., Antezana, J., Seitzman, J. M., and Lieuwen, T. C., 2009, "Global Turbulent Consumption Speeds ($S_{T,GC}$) of H_2/CO Blends," ASME Conference Proceedings, 2009(48838), pp. 559-570.

[18] Marshall, A., Venkateswaran, P., D'souza, P., Noble, D., Antezana, J., Seitzman, J., and Lieuwen, T., 2009, "Measurements of Hydrogen Blending Effects on Global Turbulent Consumption Speeds," 6th US National Combustion Meeting, pp. 11.

[19] Lipatnikov, A., and Chomiak, J., 2005, "Molecular Transport Effects on Turbulent Flame Propagation and

Structure," Progress in Energy and Combustion Science, 31(1), pp. 1-73.

[20] Karpov, V. P., Lipatnikov, A. N., and Zimont, V. L., 1997, Advances in Combustion Science: In Honor of Ya. B. Zel'dovich, AIAA, Reston, VA, Flame Curvature as a Determinant of Preferential Diffusion Effects in Premixed Turbulent Combustion.

[21] Kobayashi, H., Tamura, T., Maruta, K., Niioka, T., and Williams, F. A., 1996, "Burning Velocity of Turbulent Premixed Flames in a High-Pressure Environment," Proceedings of the Combustion Institute, 26(1), pp. 389-396.

[22] Videto, B., and Santavicca, D., 1991, "A Turbulent Flow System for Studying Turbulent Combustion Processes," Combustion Science and Technology, 76(1), pp. 159-164.

[23] Smallwood, G. J., Gülder, Ö. L., Snelling, D. R., Deschamps, B. M., and Gökalp, I., 1995, "Characterization of Flame Front Surfaces in Turbulent Premixed Methane/Air Combustion," Combustion and Flame, 101(4), pp. 461-470.

[24] Griebel, P., Siewert, P., and Jansohn, P., 2007, "Flame Characteristics of Turbulent Lean Premixed Methane/Air Flames at High Pressure: Turbulent Flame Speed and Flame Brush Thickness," Proceedings of the Combustion Institute, 31(2), pp. 3083-3090.

[25] Hanson, R. K., 1988, "Combustion Diagnostics: Planar Imaging Techniques," Proceedings of the Combustion Institute, 21(1), pp. 1677-1680.

[26] Dasch, C., 1992, "One-Dimensional Tomography- a Comparison of Abel, Onion-Peeling, and Filtered Backprojection Methods," Applied Optics, 31(8), pp. 1146–1152.

[27] Smallwood, G., and Gülder, Ö., 1995, "Characterization of Flame Front Surfaces in Turbulent Premixed Methane/Air Combustion," Combustion and Flame, 101(4), pp. 461-470.

[28] Davis, S. G., Joshi, A. V., Wang, H., and Egolfopoulos, F., 2005, "An Optimized Kinetic Model of H_2/CO Combustion," Proceedings of the Combustion Institute, 30(1), pp. 1283-1292.

[29] Smith, G. P., Golden, D. M., Frenklach, M., Moriarty, N. W., Eiteneer, B., Goldenberg, M., Bowman, C. T., Hanson, R. K., Song, S., Gardiner Jr, W. C., Lissianski, V. V., and Qin, Z., Gri-Mech 3.0, http://www.me.berkeley.edu/gri_mech/

[30] Borghi, R., 1985, "On the Structure and Morphology of Turbulent Premixed Flames," Recent advances in the aerospace sciences(A 85-47304 23-31). New York, Plenum Press, 1985, pp. 117-138.

[31] Wu, C. K., and Law, C. K., 1985, "On the Determination of Laminar Flame Speeds from Stretched Flames," Symposium (International) on Combustion, 20(1), pp. 1941-1949.

[32] Kee, R. J., Miller, J. A., Evans, G. H., and Dixon-Lewis, G., 1989, "A Computational Model of the Structure and Extinction of Strained, Opposed Flow, Premixed Methane-Air Flames," Proceedings of the Combustion Institute, 22(1), pp. 1479-1494.

[33] Poinsot, T., and Veynante, D., 2005, *Theoretical and Numerical Combustion*, RT Edwards, Inc.,

[34] Bray, K. N. C., and Cant, R. S., 1991, "Some Applications of Kolmogorov's Turbulence Research in the Field of Combustion," Proceedings: Mathematical and Physical Sciences, pp. 217-240.

[35] Damköhler, G., 1940, "The Effect of Turbulence on the Flame Velocity in Gas Mixtures," Zeitschrift Electrochem, 46(pp. 601-626.

[36] El Tahry, S. H., Rutland, C., and Ferziger, J., 1991, "Structure and Propagation Speeds of Turbulent Premixed Flames--a Numerical Study," Combustion and Flame, 83(1-2), pp. 155-173.

[37] Yuen, F. T. C., and Gülder, Ö. L., 2009, "Premixed Turbulent Flame Front Structure Investigation by Rayleigh Scattering in the Thin Reaction Zone Regime," Proceedings of the Combustion Institute, 32(2), pp. 1747-1754.

[38] Goix, P. J., and Shepherd, I. G., 1993, "Lewis Number Effects on Turbulent Premixed Flame Structure," Combustion Science and Technology, 91(4), pp. 191 - 206.

[39] Rutland, C., and Trouvé, A., 1993, "Direct Simulations of Premixed Turbulent Flames with Nonunity Lewis Numbers," Combustion and Flame, 94(1), pp. 41-57.

[40] Haworth, D. C., and Poinsot, T. J., 1992, "Numerical Simulations of Lewis Number Effects in Turbulent Premixed Flames," Journal of Fluid Mechanics, 244(pp. 405-436.

[41] Baum, M., Poinsot, T. J., Haworth, D. C., and Darabiha, N., 1994, "Direct Numerical Simulation of $H_2/O_2/N_2$ Flames with Complex Chemistry in Two-Dimensional Turbulent Flows," Journal of Fluid Mechanics, 281(pp. 1-32.

[42] Egolfopoulos, F. N., 1994, "Geometric and Radiation Effects on Steady and Unsteady Strained Laminar Flames," Proceedings of the Combustion Institute, 25(1), pp. 1375-1381.